

Maximizing tunnel magnetoresistance across three ultrathin chromium trihalides

Hyun Ho Kim^{1*}, Bowen Yang¹, Shangjie Tian², Chenghe Li², Guo-Xing Miao¹, Hechang Lei², and Adam W. Tsen^{1*}

¹*Institute for Quantum Computing, Department of Chemistry, Department of Physics and Astronomy, and Department of Electrical and Computer Engineering, University of Waterloo, Waterloo, Ontario N2L 3G1, Canada*

²*Department of Physics and Beijing Key Laboratory of Opto-electronic Functional Materials & Micro-Nano Devices, Renmin University of China, Beijing 100872, China*

*Correspondence to: hyun.kim@uwaterloo.ca, awtsen@uwaterloo.ca

Keywords: 2D magnetism, chromium trihalides, tunnel magnetoresistance

Abstract

The recent discoveries of 2D magnetism in van der Waals materials provide a novel route to realize high-performance spintronic devices. Giant tunnel magnetoresistance (TMR) as large as one million percent has recently been reported by several groups in graphene/CrI₃/graphene junctions by exploiting the weak antiferromagnetic coupling between adjacent layers. Here, we report a comparative study of TMR in all three chromium trihalides (CrX₃, X= Cl, Br, or I) in the ultrathin limit. As the materials exhibit different transition temperatures and interlayer magnetic ordering in the ground state, tunneling measurements allow for an easy determination of the field–temperature phase diagram for the three systems. By optimizing sample thickness and biasing conditions, we then demonstrate how to maximize TMR at different temperatures for each material. These results extend the prospect of 2D spintronic devices to all three chromium trihalides.

Magnetic tunnel junctions (MTJs), formed by two ferromagnetic metals separated by a thin nonmagnetic insulating barrier, and are a key building block of modern spintronic devices^{1, 2}. An important performance metric is their tunnel magnetoresistance (TMR), defined as the resistance difference between the two relative spin orientations of the ferromagnetic layers, which can be switched by an external magnetic field. While TMR values have steadily increased over time, a dramatic enhancement was seen with the use of crystalline barriers instead of amorphous layers³⁻⁵. An alternative approach to achieve large TMR is through spin filtering, whereby a *magnetic* barrier selectively tunnels electrons of a single spin polarization from *nonmagnetic* metal leads. Earlier work with deposited EuS films has shown that two spin filters with initial opposite spin polarization can generate TMR as large as 60% when the layers become fully polarized^{6, 7}. By stacking multiple spin filters with alternating polarization, one can therefore expect even larger TMR as this value compounds with increasing filter number.

The recent discoveries of 2D magnetic materials⁸⁻¹⁰, such as CrI₃, provide a novel opportunity to achieve extremely large TMR through the use of van der Waals heterostructures. CrI₃ is highly crystalline, while weak antiferromagnetic coupling between adjacent layers provide a natural series of spin filters whose TMR can be tuned by thickness and bias voltage¹¹⁻¹³. In particular, we have previously demonstrated TMR of 10⁶% in graphene/CrI₃/graphene tunnel junctions under a 2T field¹². These results motivate a systematic study of TMR in the entire CrX₃ (X= I, Br, and Cl) family across temperature and sample thickness. We observe ~1500% TMR in 15-layer (15L) CrCl₃ with antiferromagnetic (AFM) interlayer coupling at low temperature and even ~200% TMR in 8L CrBr₃ with ferromagnetic (FM) interlayer coupling near the magnetic transition temperature. These values decrease in the limit of a double filter formed in bilayers.

A schematic illustration of our devices is shown in Fig. 1a and the detailed fabrication procedure can be found in the Methods section. In short, ultrathin CrI_3 , CrBr_3 , or CrCl_3 from 2 to 15 layers (L) is exfoliated in a nitrogen-filled glovebox and sandwiched between top and bottom few-layer graphene electrodes (Gr) with full encapsulation by hexagonal boron nitride (hBN) on both sides for sample protection. In the main panel of Fig. 1b, we show an optical image of such a CrI_3 device as an example.

We begin with transport behavior without magnetic field in order to confirm the ground-state magnetic properties of CrX_3 . In Fig. 2, we show temperature-dependent I-V characteristics for few-layer devices incorporating the three different materials (CrI_3 : 8L, CrBr_3 : 8L, and CrCl_3 : 15L). All tunnel junctions exhibit nonlinear current-voltage characteristics due to quantum mechanical tunneling across the semiconducting layers. At higher bias yielding current above $\sim 1\text{nA}$, transport is governed by Fowler-Nordheim (FN) tunneling¹², while for direct tunneling near zero bias, the current is below the noise level ($\sim 1\text{pA}$) for samples of this thickness. A zero-bias conductivity is measurable in thinner samples, however (see Supplementary Fig. S1). For CrI_3 and CrCl_3 , decreasing temperature lowers the current level for a given voltage, whereas CrBr_3 shows the opposite trend. In order to verify this, we additionally measured resistance with continuously changing temperature, and the results are shown in the corresponding insets in the bottom panel of Fig. 2. Here, a marked kink (or peak) was observed at the magnetic transition temperature (T_{AFM} or T_{FM}) for each device. By taking the derivative of these curves, we determined the critical temperatures more precisely to be 46K for CrI_3 , 37K for CrBr_3 , and 17K for CrCl_3 (Supplementary Fig. S2). These temperatures are consistent with previous reports for bulk CrBr_3 ¹⁴ and CrCl_3 ¹⁵, although few-layer CrI_3 shows a slightly lower value than that for the bulk crystal (61K)¹⁶, possibly due to different interlayer spin coupling and/or stacking between the two

systems^{17, 18}. The abrupt change in tunnel resistance at the critical temperature arises from spontaneous exchange splitting of the CrX_3 bandstructure^{19, 20}. Below T_{AFM} (T_{FM}), increasing (decreasing) resistance with decreasing temperature for CrI_3 and CrCl_3 (CrBr_3) indicates that the ground-state interlayer magnetic ordering is AFM (FM) between adjacent layers, as tunneling across filters with antiparallel (parallel) spins raises (lowers) the effective barrier height. Schematic illustrations of these effects are shown in the top panel of Fig. 2. These results are consistent with several recent studies of ultrathin CrX_3 ²¹⁻²³.

The different ground-state interlayer spin ordering observed in these three materials will yield different phase transitions and TMR behavior upon application of a magnetic field, both of which can be measured in our device geometry. In Fig. 3a-c, we show voltage vs. temperature at constant current for the same three devices at several different fields applied perpendicular to the layers. We chose a small, 0.1 nA current level in order to minimize the effects of Joule heating. Nevertheless, we found that measured transition temperatures did not change up to 100nA (Supplementary Fig. S3). In general, increasing magnetic field polarizes spins parallel to the field direction. For CrI_3 and CrCl_3 , the field decreases the resistance at low temperature as the interlayer AFM ground state is gradually destroyed. For CrBr_3 , however, the low-temperature resistance is barely changed, since a spin-parallel, interlayer FM state has already formed in the ground state. Instead, the largest change occurs around the critical temperature. Here, increasing magnetic field stabilizes the parallel spin state, and so the voltage is decreased while the transition temperature into this state, T_P , is increased. This effect may be analogous to that observed in the colossal magnetoresistance manganite materials undergoing a paramagnetic (PM) insulator to FM metal transition, wherein the field suppresses the resistance caused by critical spin fluctuations or phase disorder²⁴. In CrI_3 and CrCl_3 , we observe that for intermediate magnetic fields, not only is T_P

pushed to higher temperatures, but a second transition to an antiparallel interlayer spin state can be seen at temperatures below T_{AP} and decreases for increasing field. In the limit of zero field, T_P and T_{AP} approach T_{FM} and T_{AFM} , respectively, critical temperatures for the transition to *spontaneous* magnetic order. These net results are reproducible over several different samples (see Supplementary Fig. S4). We have additionally performed field-sweep measurements at several different temperatures (see Supplementary Fig. S5). The combined dataset allows us to obtain a field-temperature phase diagram for all three materials, as shown in Fig. 3d-f. In the spin schematics for the ground state, the easy axis is drawn to be out of plane for CrI₃ and CrBr₃, while it is in-plane for CrCl₃, as had been just recently demonstrated¹⁹⁻²¹.

A field-induced transition to the spin parallel state should be accompanied by substantial TMR. In the insets of Fig. 4a-c, we show I-V plots with and without a 5.5T perpendicular field for CrI₃ and CrCl₃ at 1.4K and for CrBr₃ at 40K. When the field is applied, we generally observe clear TMR as the current is enhanced for any given voltage. For constant voltage biasing V , we define the TMR percentage between 0 and 5.5T as $\text{TMR} (\%) = \frac{I(5.5T,V) - I(0T,V)}{I(0T,V)} \times 100\%$ ⁶, and plot these voltage-dependent values in the main panels of Fig. 4a-c. First, we notice that all three devices exhibit a noticeable asymmetry between negative and positive voltage. While we are unclear as to the nature of this effect, we note that there is an inherent asymmetry built into the device geometry as the top and bottom graphite layers are not identical. Similar asymmetric behavior was also observed in previous reports^{11, 12}. Nevertheless, at an optimized voltage level, we find that TMR reaches as high as 6X10⁵% in CrI₃, 190% in CrBr₃, and 1490% in CrCl₃. For comparison, the largest TMR achieved in traditional MTJs consisting of MgO tunnel barriers is 1,010% at 5K, although for a much smaller field of 100Oe⁵. Overall, we attribute these relatively large TMR values to the high-quality interfaces naturally formed between the crystalline layers, as

well as the sizable spin splitting of the bandstructure, which we shall discuss in detail below.

First, in order to determine the smallest magnetic field necessary to achieve the large TMR, we measured current at the optimal voltage with continuously changing field. These results are shown in main panels of Fig. 4d-f. We observe that comparable TMR values can be already be achieved at 2T for CrI₃ and CrCl₃. This corresponds to the critical polarizing field for these two materials in the ground state²¹. On the other hand, TMR in the CrBr₃ device increases without saturation up to 5.5T, which is consistent with the field dependence of magnetization in the PM state. For comparison, we have also included data at 1.4K, which shows negligible TMR compared with that at 40K. We next repeated these measurements at many different temperatures and have plotted the TMR percentage for all three devices as a function of temperature in Fig. 4g. While both CrI₃ and CrCl₃ show decreasing TMR with increasing temperature, CrBr₃ shows the opposite trend up to 40K. In particular, the values for CrBr₃ and CrCl₃ cross at ~30K.

The TMR behavior in all three materials could be understood quantitatively by spin-dependent tunneling in the FN regime. Here, the current-voltage relation scales as $\ln\left(\frac{I_{\uparrow\downarrow}}{V^2}\right) \sim \frac{\Phi_{\uparrow\downarrow}^{3/2}(B)}{V}$, where $\Phi_{\uparrow\downarrow}(B)$ is the tunnel barrier for each spin species in CrX₃ and is tunable by magnetic field. For CrI₃ and CrCl₃ in the AP state, electrons of both spins encounter a spatially modulated barrier with effective height $\Phi_{\uparrow,eff}^{AP} = \Phi_{\downarrow,eff}^{AP}$. In the P state with ≥ 2 T upward field, the barrier becomes uniform, with $\Phi_{\uparrow}^P < \Phi_{eff}^{AP} < \Phi_{\downarrow}^P$. The lower barrier for spin-up electrons yields an exponential rise in spin-filtered current, which manifests as large TMR. For CrBr₃ in the PM state, increasing magnetic field instead splits the spin-degenerate barrier Φ^{PM} , with $\Phi_{\uparrow}^P < \Phi^{PM} < \Phi_{\downarrow}^P$. However, this change occurs smoothly as current increases without saturation up to 5.5T, in contrast with the abrupt change at the critical field for CrI₃ and CrBr₃. By fitting the current-

voltage data to the FN formula at different magnetic field levels and temperatures, we are able to extract all the various barrier heights as well as the size of the spin gap, $\Phi_{\downarrow}^P - \Phi_{\uparrow}^P = 2(\Phi^{PM} - \Phi_{\uparrow}^P)$ (see Supplementary Fig. S6 and S7). These quantities are shown schematically in the insets of Fig. 4d-f. CrI₃ always shows larger TMR than CrCl₃ due to greater spin splitting of the tunnel barrier relative to Φ_{eff}^{AP} . The splitting decreases with increasing temperature and gradually disappears above T_{AFM} ¹². For CrBr₃ at low temperature, increasing field has a negligible effect on the barriers since they are already split uniformly in the P state. The largest field-induced splitting instead occurs near $T_{FM} \sim 40$ K. This value is still smaller than those for CrI₃ and CrCl₃ at 1.4K, however.

Finally, we end by discussing the thickness dependence of TMR for each material at the optimized temperature (1.4K for CrI₃ and CrCl₃, and 40K for CrBr₃). In Fig. 5a, we show the maximum TMR vs. thickness for CrI₃, CrBr₃, and CrCl₃. This result shows that the TMR increases overall with increasing barrier thickness, a consequence of multiple spin filters acting in series. Furthermore, TMR in CrI₃ has the strongest change from 2 to 6 layers, as had also been reported previously¹¹⁻¹³, and saturates in thicker samples. In contrast, CrCl₃ and CrBr₃ devices show a more gradual increase. Taken together, these results show that few-layer samples above 6 layers are more ideal to obtain higher TMR in all three chromium trihalides.

In summary, we have investigated the magnetic properties of all three chromium halides in the atomically thin limit by incorporating them in van der Waals tunnel junctions. We have characterized both the ground state and field-driven phases as well as their TMR behavior. By optimizing for sample thickness, bias voltage, and temperature, we demonstrate how to maximize TMR for each material, an important device performance metric. Our work will have important implications for future spintronic devices utilizing these 2D materials.

Methods

Crystal synthesis. CrI₃ and CrCl₃ single crystals were grown by the chemical vapor transport method. We used a two-zone horizontal tube furnace. The temperature for source (growth) zones was gradually raised to 993 – 873K (823 – 723K) within 24 hours, and then held for 150 hours for actual growth. CrBr₃ single crystals was purchased from HQ graphene.

Device fabrication. Graphite (CoorsTek), h-BN (HQ graphene), CrI₃, CrBr₃ (HQ graphene), and CrCl₃ were exfoliated onto SiO₂(285nm)/Si chip within a nitrogen-filled glove box (Inert Pure LabHE, $P_{O_2}, P_{H_2O} < 0.1\text{ppm}$). By using a polymer-assisted pickup method reported previously²⁵, we sequentially stacked the structure of hBN/graphite/CrX₃/graphite/hBN in a home-built transfer setup inside the glove box, followed by transferring whole stack onto pre-patterned Au (40nm)/Ti (5nm) electrodes produced by conventional photolithography & lift-off methods and e-beam deposition. The overlapping area of graphite/CrX₃/graphite was set to be $\sim 10 \mu\text{m}^2$ for few-layer devices and $\sim 1 \mu\text{m}^2$ for bilayer devices. 1.4- and 7- nm-thick CrI₃ (2, 4, 8, and 10L), 1.3- to 7.8- nm-thick CrBr₃ (2, 8, 10, and 12L), and 1.2- to 9-nm-thick CrCl₃ (2, 8, 10, 12 and 15L) were used for fabrication. Gr electrodes were connected with each pre-patterned electrodes and hBN layers were used as protecting layers. Devices were stored inside the glovebox until they were loaded into the cryostat.

Acknowledgements

AWT acknowledges support from an NSERC Discovery grant (RGPIN-2017-03815), an Ontario Early Researcher Award (ER17-13-199), and the Korea-Canada Cooperation Program through the National Research Foundation of Korea (NRF) funded by the Ministry of Science, ICT and Future

Planning (NRF-2017K1A3A1A12073407). G-XM acknowledges support from an NSERC Discovery grant (RGPIN-04178). This research was undertaken thanks in part to funding from the Canada First Research Excellence Fund. HCL acknowledges support from the National Key R&D Program of China (Grants No. 2016YFA0300504), the National Natural Science Foundation of China (No. 11574394, 11774423, 11822412), the Fundamental Research Funds for the Central Universities, and the Research Funds of Renmin University of China (RUC) (15XNLQ07, 18XNLG14, 19XNLG17).

Competing interests

The authors declare no competing interests.

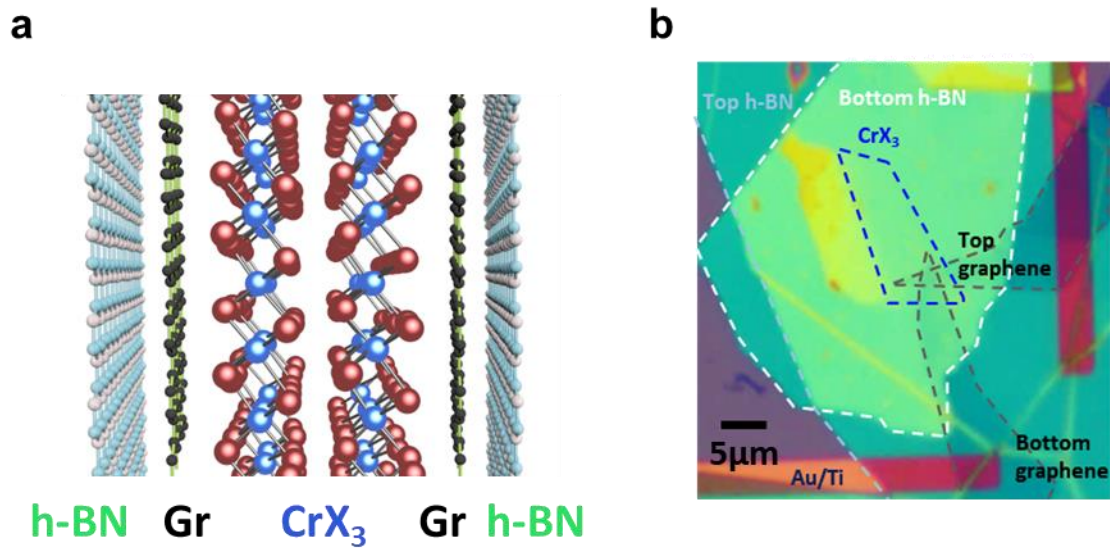


Figure 1. Van der Waals tunnel junctions incorporating ultrathin magnetic chromium trihalides. (a) Schematic illustration of the device. (b) Example optical image of a completed device with 2L CrI₃.

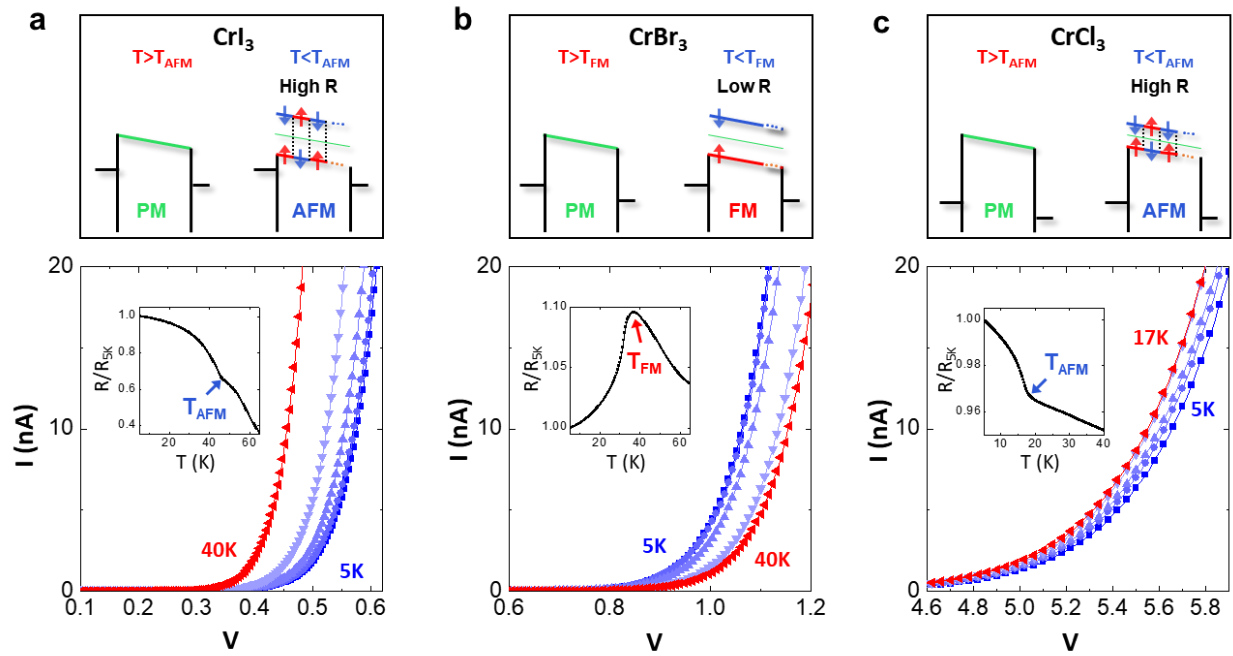


Figure 2. Temperature-dependent I-V measurement of (a) 8-layered CrI_3 (5, 10, 20, 30, and 40K), (b) 8-layered CrBr_3 (5, 10, 20, 30, and 40K), and (c) 15-layered CrCl_3 (5, 12, 14, 16, and 17K) at 0T. Insets show temperature-dependent, normalized d.c. resistance at 0T. Top panel shows respective, spin-dependent energy band diagrams of Gr/ CrX_3 /Gr tunnel junctions above and below the magnetic transition temperature.

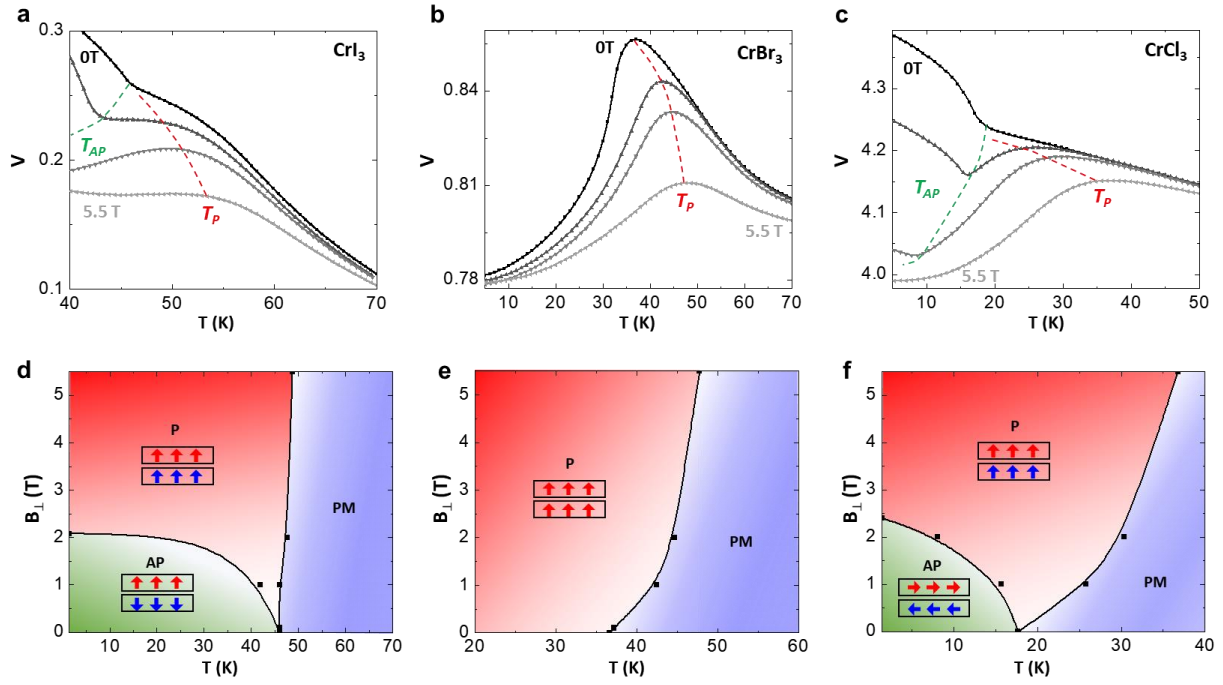


Figure 3. Tunneling probe of interlayer magnetic phases for three ultrathin chromium trihalides. (a) Voltage vs. temperature at 0.1 nA current biasing of a) 8-layer CrI_3 , (b) 8-layer CrBr_3 , and (c) 15-layer CrCl_3 for different B_{\perp} (0, 1, 2, and 5.5 T, in sequence from top) (d-f) Field-temperature phase diagram obtained from (a-c).

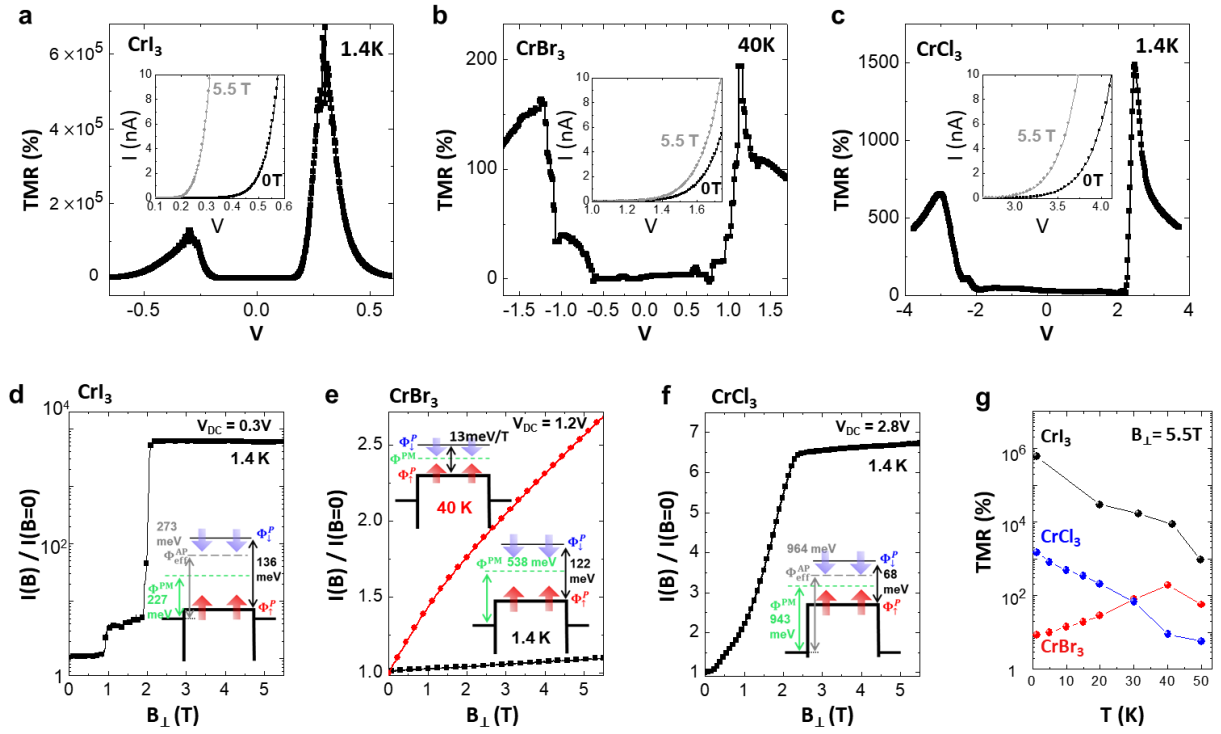


Figure 4. Tunnel magnetoresistance in three ultrathin chromium trihalides. TMR vs. voltage at 5.5T for in (a) 8-layer CrI₃ (1.4K), (b) 12-layer CrBr₃ (40K), and (c) 12-layer CrCl₃ (1.4K). Insets in (a-c) show full I-V characteristics at 0T and $B_{\perp} = 5.5\text{T}$ for the same devices. (d-f) Normalized tunnel current versus perpendicular magnetic field for the same devices. Insets in (d-f) show extracted spin-dependent energy band diagrams for CrX₃. (g) Temperature-dependent, TMR at optimized voltage at $B_{\perp} = 5.5\text{T}$.

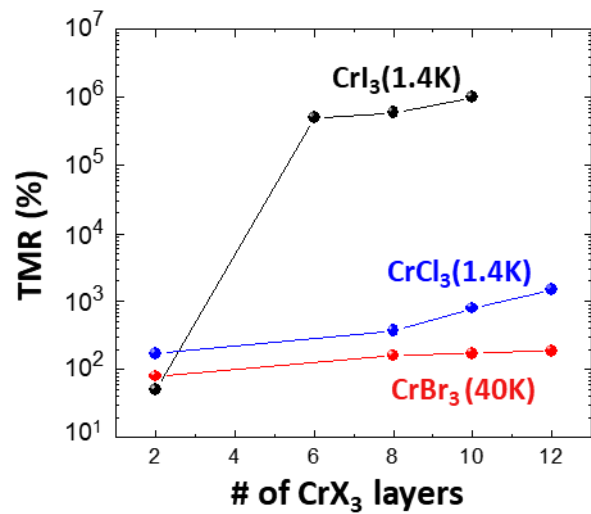


Figure 5. Maximum TMR of CrX₃ as a function of the number of layers.

References

1. Wolf, S. A.; Awschalom, D. D.; Buhrman, R. A.; Daughton, J. M.; von Molnár, S.; Roukes, M. L.; Chtchelkanova, A. Y.; Treger, D. M. Spintronics: A Spin-Based Electronics Vision for the Future. *Science* **2001**, *294* (5546), 1488.
2. Žutić, I.; Fabian, J.; Das Sarma, S. Spintronics: Fundamentals and applications. *Rev. Mod. Phys.* **2004**, *76* (2), 323-410.
3. Yuasa, S.; Nagahama, T.; Fukushima, A.; Suzuki, Y.; Ando, K. Giant room-temperature magnetoresistance in single-crystal Fe/MgO/Fe magnetic tunnel junctions. *Nat. Mater.* **2004**, *3* (12), 868-871.
4. Parkin, S. S. P.; Kaiser, C.; Panchula, A.; Rice, P. M.; Hughes, B.; Samant, M.; Yang, S.-H. Giant tunnelling magnetoresistance at room temperature with MgO (100) tunnel barriers. *Nat. Mater.* **2004**, *3* (12), 862-867.
5. Lee, Y. M.; Hayakawa, J.; Ikeda, S.; Matsukura, F.; Ohno, H. Effect of electrode composition on the tunnel magnetoresistance of pseudo-spin-valve magnetic tunnel junction with a MgO tunnel barrier. *Appl. Phys. Lett.* **2007**, *90* (21), 212507.
6. Miao, G.-X.; Müller, M.; Moodera, J. S. Magnetoresistance in Double Spin Filter Tunnel Junctions with Nonmagnetic Electrodes and its Unconventional Bias Dependence. *Phys. Rev. Lett.* **2009**, *102* (7), 076601.
7. Gao, Z.; Yang, Y.; Liu, F.; Xue, Q.; Miao, G.-X. Spin- and symmetry-filtering combined tunnel magnetoresistance through epitaxial MgO/EuS tunnel barriers. *Mater. Res. Express* **2016**, *3* (7), 075017.
8. Gong, C.; Li, L.; Li, Z.; Ji, H.; Stern, A.; Xia, Y.; Cao, T.; Bao, W.; Wang, C.; Wang, Y.; et al. Discovery of intrinsic ferromagnetism in two-dimensional van der Waals crystals. *Nature* **2017**, *546*, 265-269.
9. Huang, B.; Clark, G.; Navarro-Moratalla, E.; Klein, D. R.; Cheng, R.; Seyler, K. L.; Zhong, D.; Schmidgall, E.; McGuire, M. A.; Cobden, D. H.; et al. Layer-dependent ferromagnetism in a van der Waals crystal down to the monolayer limit. *Nature* **2017**, *546*, 270-273.
10. Deng, Y.; Yu, Y.; Song, Y.; Zhang, J.; Wang, N. Z.; Wu, Y. Z.; Zhu, J.; Wang, J.; Chen, X. H.; Zhang, Y. Gate-tunable Room-temperature Ferromagnetism in Two-dimensional Fe₃GeTe₂. *Nature* **2018**, *563*, 94-99.
11. Song, T.; Cai, X.; Tu, M. W.-Y.; Zhang, X.; Huang, B.; Wilson, N. P.; Seyler, K. L.; Zhu, L.; Taniguchi, T.; Watanabe, K.; et al. Giant tunneling magnetoresistance in spin-filter van der Waals heterostructures. *Science* **2018**, *360*, 1214-1218.
12. Kim, H. H.; Yang, B.; Patel, T.; Sfigakis, F.; Li, C.; Tian, S.; Lei, H.; Tsen, A. W. One million percent tunnel magnetoresistance in a magnetic van der Waals heterostructure. *Nano Lett.*

2018, *18*, 4885-4890.

13. Wang, Z.; Gutiérrez-Lezama, I.; Ubrig, N.; Kroner, M.; Taniguchi, T.; Watanabe, K.; Imamoğlu, A.; Giannini, E.; Morpurgo, A. F. Very Large Tunneling Magnetoresistance in Layered Magnetic Semiconductor CrI₃. *Nat. Commun.* **2018**, *9*, 2516.

14. Tsubokawa, I. On the Magnetic Properties of a CrBr₃ Single Crystal. *J. Phys. Soc. Jpn.* **1960**, *15* (9), 1664-1668.

15. McGuire, M. A.; Clark, G.; Kc, S.; Chance, W. M.; Jellison, G. E.; Cooper, V. R.; Xu, X.; Sales, B. C. Magnetic behavior and spin-lattice coupling in cleavable van der Waals layered CrCl₃ crystals. *Phys. Rev. Mater.* **2017**, *1* (1), 014001.

16. McGuire, M. A.; Dixit, H.; Cooper, V. R.; Sales, B. C. Coupling of Crystal Structure and Magnetism in the Layered, Ferromagnetic Insulator CrI₃. *Chem. Mater.* **2015**, *27* (2), 612-620.

17. Sivadas, N.; Okamoto, S.; Xu, X. D.; Fennie, C. J.; Xiao, D. Stacking-Dependent Magnetism in Bilayer CrI₃. *Nano Lett.* **2018**, *18* (12), 7658-7664.

18. Jiang, P.; Wang, C.; Chen, D.; Zhong, Z.; Yuan, Z.; Lu, Z.-Y.; Ji, W. Stacking tunable interlayer magnetism in bilayer CrI₃. *Phys. Rev. B* **2019**, *99* (14), 144401.

19. Lado, J. L.; Fernández-Rossier, J. On the origin of magnetic anisotropy in two dimensional CrI₃. *2D Mater.* **2017**, *4* (3), 035002.

20. Zhang, W.-B.; Qu, Q.; Zhu, P.; Lam, C.-H. Robust intrinsic ferromagnetism and half semiconductivity in stable two-dimensional single-layer chromium trihalides. *J. Mater. Chem. C* **2015**, *3* (48), 12457-12468.

21. Kim, H. H.; Yang, B.; Li, S.; Jiang, S.; Jin, C.; Tao, Z.; Nichols, G.; Sfigakis, F.; Zhong, S.; Li, C.; et al. Evolution of interlayer and intralayer magnetism in three atomically thin chromium trihalides. **2019**, preprint at <https://arxiv.org/abs/1903.01409>.

22. Klein, D. R.; MacNeill, D.; Song, Q.; Larson, D. T.; Fang, S.; Xu, M.; Ribeiro, R. A.; Canfield, P. C.; Kaxiras, E.; Comin, R.; et al. Giant enhancement of interlayer exchange in an ultrathin 2D magnet. **2019**, preprint at <https://arxiv.org/abs/1903.00002>.

23. Cai, X.; Song, T.; Wilson, N. P.; Clark, G.; He, M.; Zhang, X.; Taniguchi, T.; Watanabe, K.; Yao, W.; Xiao, D.; et al. Atomically Thin CrCl₃: An in-Plane Layered Antiferromagnetic Insulator. **2019**, preprint at <https://arxiv.org/abs/1904.00261>.

24. Ramirez, A. P. Colossal magnetoresistance. *J. Phys. Condens. Matter.* **1997**, *9* (39), 8171-8199.

25. Wang, L.; Meric, I.; Huang, P. Y.; Gao, Q.; Gao, Y.; Tran, H.; Taniguchi, T.; Watanabe, K.; Campos, L. M.; Muller, D. A.; et al. One-Dimensional Electrical Contact to a Two-Dimensional Material. *Science* **2013**, *342* (6158), 614-617.